

Emergent chiral symmetry in non-bipartite kagome and pyrochlore lattices with spin-orbit coupling

Hiroki Nakai^{1,*}, Masataka Kawano^{1,2}, and Chisa Hotta^{1†}

¹*Department of Basic Science, University of Tokyo, Meguro-ku, Tokyo 153-8902, Japan and*

²*Department of Physics, Technical University of Munich, 85748 Garching, Germany*

(Dated: August 16, 2022)

Chiral symmetry in energy bands appears as perfectly symmetric anti-bonding and bonding pairs of energy levels. It has only been observed in a few classes of models with a bipartite lattice structure or Bogoliubov-de-Gennes systems having the pairwise basis. We show that the *non-bipartite* kagome and pyrochlore lattices can host chiral symmetric bands when the strong spin-orbit coupling is introduced. There, the electrons hop to their neighbors by always converting the spin orientation up-side-down, which allows the up and down spin bases to form fictitious bipartite connections. The gauge invariant Wilson loop operator defined on a triangular unit serves as a marker to detect the presence of chiral symmetry, and using this property, the chiral operator is constructed. This allows us to access their topological symmetry classes that can easily change with small perturbations.

Introduction. Possible types of electronic phases of matter are very often discussed and tabulated in terms of symmetries. The space group symmetries combined with time-reversal symmetry (TRS) determines the types of electronic band structures and the possible choices of symmetry broken phases out of them [1, 2]. On the other hand, the periodic table developed for topological insulators (TI) and superconductors has revealed that the symmetries that protect them and distinguish them from are not the spatial ones but are the TRS, particle-hole symmetry (PHS) and chiral symmetry (CS) [3, 4]. The CS is identified as the diphycercal shape of positive and negative parts in the energy spectrum and is present when the TRS and the PHS are both broken or both unbroken. These three symmetries generate a total of ten symmetry classes, which are extended through the combination with spatial symmetries [5].

The CS serves as a guide to elucidate the nature of topological phases [6]. For example, the winding number in the Su-Schrieffer-Heeger model [7–9] is defined using the CS operator, and the number of singular zero-mode Landau level and the bulk-edge correspondence of graphene [10–12] are understood by this symmetry. It explains the stable zero modes of bilayer graphene [13, 14], and when combined with spatial symmetry, it further protects the extra topological zero modes, showing us how many independent topological invariants are required to describe that state [15].

Despite its importance, the CS is observed only in restricted classes of models; they are the bipartite hopping model [16] and its analogues [17, 18], the quadratic low energy effective Hamiltonian obeying the Bogoliubov-de-Gennes (BdG) equations with TRS and conserved magnetization, and the QCD models [19]. How this symmetry could emerge in wider classes of physical systems is an important question. Here, we discover that the noninteracting fermions on a *non-bipartite* lattice with strong spin-orbit coupling (SOC) can host a CS band structure. We further prove that the gauge invariant Wilson loop

operator [20] serves as a detector of the CS, and using the Wilson loop operator, obtain an explicit form of the chiral operator. We show that several realistic types of perturbation to the CS energy bands will easily transform it from class DIII to various other classes in the topological periodic table; CS can be preserved or gives rise to the strong TI with apparent edge states.

Chiral symmetry. Without the loss of generality, the low energy effective Hamiltonian in momentum space is described by the quadratic Hamiltonian given as $\mathcal{H} = \sum_{\mathbf{k}} \mathbf{c}_{\mathbf{k}}^{\dagger} \mathcal{H}(\mathbf{k}) \mathbf{c}_{\mathbf{k}}$, where $\mathbf{c}_{\mathbf{k}}^{\dagger} = (c_{\mathbf{k}1\uparrow}^{\dagger}, c_{\mathbf{k}1\downarrow}^{\dagger}, \dots, c_{\mathbf{k}n\uparrow}^{\dagger}, c_{\mathbf{k}n\downarrow}^{\dagger})$ are the set of creation operators of a Bloch electron with spin (\uparrow, \downarrow) and wavevector \mathbf{k} on the sublattice index $l = (1, 2, \dots, n)$, and the Bloch Hamiltonian $\mathcal{H}(\mathbf{k})$ is the $2n \times 2n$ Hermitian matrix. If the energy bands, $\pm E_m(\mathbf{k})$, obtained by diagonalizing $\mathcal{H}(\mathbf{k})$ is symmetric about the central zero energy level, there should exist a chiral operator Γ that satisfies $\Gamma \mathcal{H}(\mathbf{k}) \Gamma^{\dagger} = -\mathcal{H}(\mathbf{k})$. In the basis that makes Γ diagonal, the operators are represented as

$$\Gamma = \begin{pmatrix} I & 0 \\ 0 & -I \end{pmatrix}, \quad \mathcal{H}(\mathbf{k}) = \begin{pmatrix} 0 & D(\mathbf{k}) \\ D^{\dagger}(\mathbf{k}) & 0 \end{pmatrix}, \quad (1)$$

where $D(\mathbf{k})$ is the $n_1 \times n_2$ matrix in general, and there are at least $|n_1 - n_2|$ zero modes. While for our Hamiltonian, we always find $n_1 = n_2 = n$. The eigenvectors of $\Gamma = \pm 1$ are described in the form, $(\boldsymbol{\alpha}_m(\mathbf{k}), \mathbf{0})^T$ and $(\mathbf{0}, \boldsymbol{\beta}_m(\mathbf{k}))^T$. Then, the energy eigenstates are their bonding or anti-bonding states given as

$$|\psi_{\pm m}(\mathbf{k})\rangle \propto \begin{pmatrix} \boldsymbol{\alpha}_m(\mathbf{k}) \\ \mathbf{0} \end{pmatrix} \pm \begin{pmatrix} \mathbf{0} \\ \boldsymbol{\beta}_m(\mathbf{k}) \end{pmatrix}, \quad (2)$$

and Γ interchanges them. The reason why we find a CS in the bipartite and BdG systems is that due to the equivalence of two sublattices or the superconducting pairs, the Bloch basis is trivially classified into two equivalent groups that have $\Gamma = \pm 1$. For our non-bipartite lattice, the up and down spins take this role, whereas remarkably, such spin-based CS does not necessarily require the spin-conversion-symmetry represented by TRS.

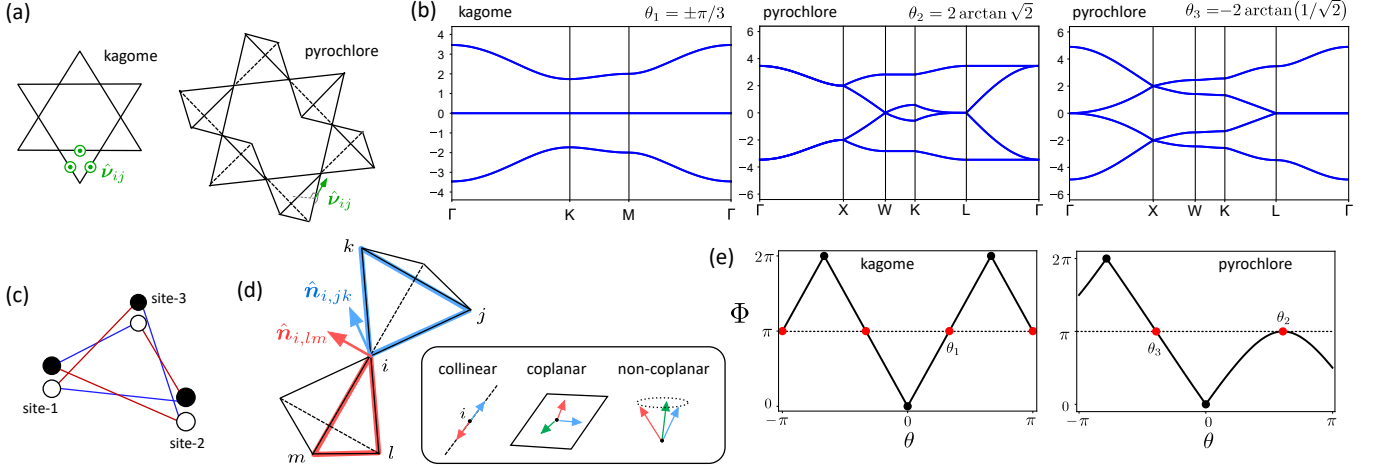


FIG. 1. (a) Kagome and pyrochlore lattices. The rotation axis $\hat{\nu}_{ij}$ of the SU(2) gauge field is shown. (b) The chiral symmetric band structures are shown at $\theta = \theta_1 = \pm\pi/3$ and $\pm\pi$ for the kagome lattice and $\theta_2 = 2 \arctan \sqrt{2}$, $\theta_3 = -2 \arctan(1/\sqrt{2})$ for the pyrochlore lattice, where $\lambda/t_0 = \tan(\theta/2)$. (c) Schematic illustration of the fictitious bipartite structure on a triangle. The up/down spins are represented by black/white circles, respectively, and the different spins are connected. (d) The Wilson loop operator rotates the spins when hopping around the $C_{i,jk}$ loop by Φ about the $\hat{n}_{i,jk}$ -axis. (e) Φ for the kagome and pyrochlore lattices. At CS points, $\theta_1, \theta_2, \theta_3$, we find $\Phi = \pi$.

SOC Hamiltonian on a non-bipartite lattice. We consider a tight-binding Hamiltonian defined on the kagome and pyrochlore lattices given as

$$\mathcal{H} = -t \sum_{\langle i,j \rangle} \mathbf{c}_i^\dagger U_{ij} \mathbf{c}_j + \text{h.c.}, \quad (3)$$

where $\mathbf{c}_i = (c_{i\uparrow}, c_{i\downarrow})^T$ is the annihilation operator of an electron at site- i , and the summation is taken over the neighboring pairs of sites, $\langle i, j \rangle$. $\boldsymbol{\sigma} = (\sigma_x, \sigma_y, \sigma_z)$ are Pauli matrices and the hopping amplitude is set to unity, $t = 1$. When the electron hops from site- j to the nearby site- i , its spin rotates by angle θ about the $\hat{\nu}_{ij}$ -axis, which is expressed by the SU(2) gauge field $U_{ij} = \exp[-i\frac{\theta}{2}\hat{\nu}_{ij} \cdot \boldsymbol{\sigma}]$, where $\hat{\nu}_{ji} = -\hat{\nu}_{ij}$ and $U_{ji} = U_{ij}^\dagger$. The unit vector $\hat{\nu}_{ij}$ is determined by the lattice symmetry, and points to the direction perpendicular to the plane for the kagome lattice [21], while points in different directions perpendicular to the bond i - j for the pyrochlore lattice [22] (see Fig.1(a) and Supplementary A). The origin of the SU(2) gauge field is the SOC [23–26]; In many 4d and 5d-electron systems, the interplay of strong *atomic* SOC and the crystal field enforces the reconstruction of energy levels on each site, and often the Kramers doublets labeled by the spin-index σ form the valence bands [27–30]. Examples in pyrochlore oxides that form such doublets are d^5 systems, $A_2\text{Ir}_2\text{O}_7$ [31–34] and $\text{Lu}_2\text{Rh}_2\text{O}_7$ [35]. In addition, $A_2\text{Os}_2\text{O}_7$ [36, 37] and CsW_2O_6 [38] of different valences also belong to this category in the presence of a trigonal crystal field [29, 39]. Since the spin momentum $\boldsymbol{\sigma}$ is the combination of orbital angular momentum and electron-spin momentum,

the electrons can hop between orbitals having different spins as, $i\lambda c_{i\alpha}^\dagger (\hat{\nu}_{ij} \cdot \boldsymbol{\sigma})_{\alpha\beta} c_{j\beta}$. By combining this spin-dependent hopping term with the ordinary hopping term, $-t_0 c_{i\alpha}^\dagger c_{j\alpha}$, the form Eq.(3) is obtained as $t = \sqrt{t_0^2 + \lambda^2}$ and $\theta = 2 \arctan(\lambda/t_0)$.

SOC induced chiral symmetry. As shown in Fig.1 (b), the energy band structures of Eq.(3) have CS at $\theta_1 = \pm\pi/3, \pm\pi$ for the kagome lattice and $\theta_2 = 2 \arctan \sqrt{2}, \theta_3 = -2 \arctan(1/\sqrt{2})$ for the pyrochlore lattice. To understand its origin, we need to find the form of two groups of basis sets that give $\Gamma = \pm 1$ in Eq.(1). Since both lattices consist of triangles, the basis set transformed back to the real space from the $\Gamma = \pm 1$ Bloch basis should be such that they have a finite hopping element between the neighboring sites only between different spin orientations. If such construction is possible, the up-spin electron on site-1 hops to site-2 and to site-3 by flipping its spin each time, and comes back to site-1 as a down-spin electron, as shown in Fig.1 (c). If we go around the triangle twice, the initial spin orientation is recovered. This picture turns out to be valid when we construct the chiral operator.

Gauge invariants. We now define a parameter that detects the CS. To do so, we need to characterize the nature of the SU(2) gauge that this symmetry relies on. However, the explicit form of U_{ij} , namely θ and $\hat{\nu}_{ij}$ change if we apply the local gauge transformation: $\mathbf{c}_i \rightarrow V_i \mathbf{c}_i$, where V_i denotes the SU(2) rotation of the quantized axis at site- i . This change is only a matter of representation and the band structure is gauge invariant. Accordingly, the parameter that characterizes the band structure should also be gauge invariant, for which we

choose the Wilson loop operator:

$$P(C_{i,jk}) = U_{ik}U_{kj}U_{ji} = \exp \left[-i \frac{\Phi}{2} \hat{\mathbf{n}}_{i,jk} \cdot \boldsymbol{\sigma} \right], \quad (4)$$

constructed by the path-ordered product of SU(2) gauge field along the closed loop $C_{i,jk} : i \rightarrow j \rightarrow k \rightarrow i$ (see Fig.1 (d)). When the electron circles along the loop $C_{i,jk}$, its spin orientation experiences a Φ rotation about the $\hat{\mathbf{n}}_{i,jk}$ -axis. Figure 1 (e) shows Φ as a function of θ for kagome and pyrochlore lattices. By comparing it with the band structures, we find that the CS is characterized by $\Phi = \pi$. For the kagome lattice, Φ and band structures are the same between $\pm\theta$, but not for the pyrochlore lattice. This is because $\hat{\mathbf{v}}_{ij}$ is common to all bonds for the former and not for the latter, and accordingly, the U_{ij} of different bonds are commutative/noncommutative for the former/latter, which we denote the Abelian/non-Abelian case. We comment that these two should be rigorously distinguished as such that there exists a gauge that makes the SU(2) gauge fields commutative in the Abelian case and no such gauge in the non-Abelian case. If the definition of non-Abelian depends on the choice of gauge [40], it does not give particular difference from the Abelian case about the gauge-invariant band structures or topological properties (see Supplementary B). When $\Phi = 2\pi$, the flat-band is formed by the SOC in both lattices [39].

For the non-Abelian case, there should be another gauge-invariant quantity that distinguishes the positive and negative θ , which is the scalar product $\hat{\mathbf{n}}_{i,jk} \cdot \hat{\mathbf{n}}_{i,lm}$ around site- i defined for different loops, $C_{i,jk}$ and $C_{i,lm}$. Although $\hat{\mathbf{n}}_{i,jk}$ is not gauge invariant, their relative angle is invariant (see Fig. 1(d) and proof in Supplementary B) [20]. Using this fact, we can classify the states into four, which we call trivial, collinear, coplanar, and non-coplanar cases. For the trivial case, $\Phi = 0, 2\pi$, the axis $\hat{\mathbf{n}}_{i,jk}$ is not defined since $P(C_{i,jk}) \propto I$. For $\Phi \neq 0, 2\pi$, if all $\hat{\mathbf{n}}_{i,jk}$ with different jk 's for the same i are parallel we call it collinear, or if they are in the same plane we call it coplanar, and otherwise, it is non-coplanar (see the inset of Fig. 1(d)). When the system is Abelian, it corresponds to either a collinear or trivial case. The non-Abelian case can be examined by comparing the two CS in Fig. 1(b): θ_2 is collinear and θ_3 is coplanar.

Chiral operator. The general form of the local gauge transformation is $V_j = \exp \left[-i \frac{\varphi_j}{2} \hat{\mathbf{m}}_j \cdot \boldsymbol{\sigma} \right]$, which rotates the spin quantization axis at site- j by an angle φ_j about the axis $\hat{\mathbf{m}}_j$. If one could find the particular form of V_j that fulfills

$$V_i U_{ij} V_j^\dagger = -U_{ij}, \quad (5)$$

one can construct a chiral operator satisfying $\Gamma^2 = +I$ as

$$\Gamma = \bigoplus_{j=1}^n i V_j, \quad (6)$$

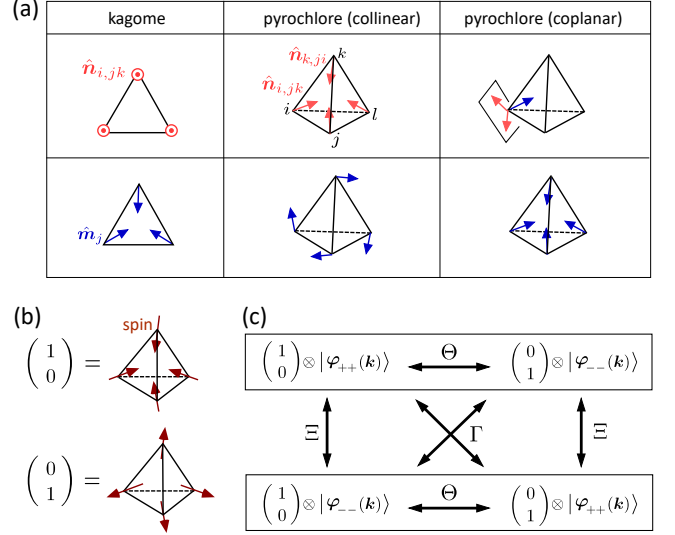


FIG. 2. (a) Vectors $\hat{\mathbf{n}}_{i,jk}$ and $\hat{\mathbf{m}}_j$ on the kagome and pyrochlore lattices with CS. (b) All-in and all-out spin configurations forming a chiral pair. (c) Relationships of four different energy eigenstates of the pyrochlore bands (collinear type CS) that interchange by the TRS, PHS, and CS operations.

for which we immediately find $\Gamma \mathcal{H}(\mathbf{k}) \Gamma^\dagger = -\mathcal{H}(\mathbf{k})$. To find such V_j we focus on the fact that the Wilson loop operator in Eq.(4) is obtained by the product of three U_{ij} 's. Accordingly, the chiral operation that changes the sign of U_{ij} 's will change the sign of $P(C_{i,jk})$. Since $\Phi = \pi$ at the CS point, the sign-change is attained by the conversion of the axis via Eq.(5) as $\hat{\mathbf{n}}_{i,jk} \rightarrow -\hat{\mathbf{n}}_{i,jk}$. Namely, we need to set $\varphi_i = \pi$ and $\hat{\mathbf{m}}_i \perp \hat{\mathbf{n}}_{i,jk}$ for all different $C_{i,jk}$'s around site- i . It follows that $\hat{\mathbf{m}}_i$ can be defined when and only when $\hat{\mathbf{n}}_{i,jk}$'s on site- i are either collinear or coplanar. To summarize, the chiral operator Γ that satisfies Eq.(1) can be constructed when the Wilson loop operators satisfy: (i) $\Phi = \pi$, (ii) $\hat{\mathbf{n}}_{i,jk}$ is collinear or coplanar, where we can write down the explicit form the form as $iV_j = \hat{\mathbf{m}}_j \cdot \boldsymbol{\sigma}$.

Figure 2(a) shows the actual directions of $\hat{\mathbf{m}}_j$ for three different CS. Then, Eq. (6) indicates that in the basis that diagonalizes Γ , the up/down spin under the local quantization axis is parallel/antiparallel to $\hat{\mathbf{m}}_j$. Because of the block-off-diagonal form of the Hamiltonian in Eq.(1), the electrons always turnover their spins when hopping. Namely, the up/down spin basis forms a fictitious bipartite connection which we discussed in Fig. 1(c).

Emergent sublattice pseudospins. In describing the CS Hamiltonian, Eq.(1), we find $D^\dagger(\mathbf{k}) \neq D(\mathbf{k})$ in general, but our collinear case shows $D^\dagger(\mathbf{k}) = D(\mathbf{k})$ (Supplementary C). Then, for $\varphi_m(\mathbf{k})$ that satisfies $D(\mathbf{k})\varphi_m(\mathbf{k}) = E_m\varphi_m(\mathbf{k})$, we find $\mathcal{H}(\mathbf{k})|\psi_{\pm m}(\mathbf{k})\rangle = \pm E_m|\psi_{\pm m}(\mathbf{k})\rangle$, with $|\psi_{\pm m}(\mathbf{k})\rangle$ in Eq.(2) having $\boldsymbol{\alpha}_m(\mathbf{k}) = \boldsymbol{\beta}_m(\mathbf{k}) = \varphi_m(\mathbf{k})$.

Reminding that the spin quantization axis for the CS basis is parallel to $\hat{\mathbf{m}}_j$ pointing toward the center of the triangle or tetrahedron, the eigenstates are the bonding and anti-bonding combinations of the all-in and all-out spin configurations shown in Fig. 2(b). In this construction, the sublattice(orbital) degrees of freedom in $D(\mathbf{k})$ show some hidden symmetries; For the kagome lattice,

$$D(\mathbf{k}) = \mathbf{R}(\mathbf{k}) \cdot \mathbf{S}, \quad (7)$$

where \mathbf{S} is the spin-1 operator in the 3×3 matrix representation (see Supplementary C). The eigenstate $\varphi_m(\mathbf{k})$ of the sublattice degrees of freedom has three states with $S = 1, 0, -1$. The energy bands carry the sublattice pseudospins that point parallel/antiparallel to the SO(3) vector $\mathbf{R}(\mathbf{k})$ whose direction varies with k , which reminds us of a Rashba-Dresselhaus Hamiltonian [41, 42].

For the pyrochlore lattice,

$$D(\mathbf{k}) = \mathbf{R}_1(\mathbf{k}) \cdot \mathbf{S}_1 + \mathbf{R}_2(\mathbf{k}) \cdot \mathbf{S}_2, \quad (8)$$

where $\mathbf{R}_j(\mathbf{k})$ is the three-dimensional vector. \mathbf{S}_1 and \mathbf{S}_2 are the spin-1/2 operators, which commute with each other in the 4×4 matrix representation (Supplementary C). We find four eigenstates $\varphi_m(\mathbf{k})$ depending on whether \mathbf{S}_1 and \mathbf{S}_2 are parallel or antiparallel to $\mathbf{R}_1(\mathbf{k})$ and $\mathbf{R}_2(\mathbf{k})$, which we denote as $\varphi_{\sigma_1\sigma_2}(\mathbf{k})$ ($\sigma_i = \pm$), and its eigenvalue is $(\sigma_1|\mathbf{R}_1(\mathbf{k})| + \sigma_2|\mathbf{R}_2(\mathbf{k})|)/2$.

We briefly mention a few points about the chiral zero modes. The doubly degenerate chiral flat band of the kagome lattice appears because n is odd [43], differently from the Lieb lattice having $n_1 \neq n_2$ in Eq.(1). For the pyrochlore lattice, the W and L point contacts for θ_2 and the Γ -L nodal line for θ_3 are the essential degeneracies [44] protected by the CS and lattice symmetry (see Supplementary C using Eq.(8)).

Symmetries and perturbations. How the TRS, PHS, and CS act on the energy eigenstates of the pyrochlore lattice at $\theta = \theta_2$ is shown in Fig. 2(c). Γ flips the true spin but not the sublattice pseudospin (σ_1, σ_2), and interchanges the energy level $\pm E_m$. Ξ flips only the sublattice spins and interchanges $\pm E_m$. Θ flips both and exchanges the energetically degenerate pairs of states. It then follows that if the system has the CS and TRS, it also has PHS, reproducing $\Xi = \Gamma\Theta$. Since Γ is expressed as in Eq.(6), $\Theta^{-1}\Gamma\Theta = -\Gamma$, which indicates that $\Xi^2 = +I$. Reminding that Ξ takes the role of pseudo-TRS for sublattice pseudospins, $\Xi^2 = +I$ prohibits the odd-numbered half-integer sublattice pseudospins. This explains why Eq.(8) is not described by a single pseudospin-3/2 but by the two pseudospin-1/2.

Another interest is how robust is our CS against the perturbations that may commonly appear in the actual material systems. Using the Wilson loop operator, we examine three types of perturbations as shown in Table I (see Supplementary D). The magnetic field (Zeeman terms) breaks both TRS and PHS, and for a particular

TABLE I. The effect of perturbations on TRS, PHS, and CS. The absence of symmetry is denoted as 0, and the presence of TRS or PHS is denoted as ± 1 according to $\Theta^2, \Xi^2 = \pm I$, and that of CS as 1. The last column shows the symmetry class the Hamiltonian belongs to [3].

perturbation	TRS	PHS	CS	AZ class
magnetic field	0	0	0/1	A/AIII
on-site potential	-1	0	0	AII
bond modulation	-1	+1	1	DIII

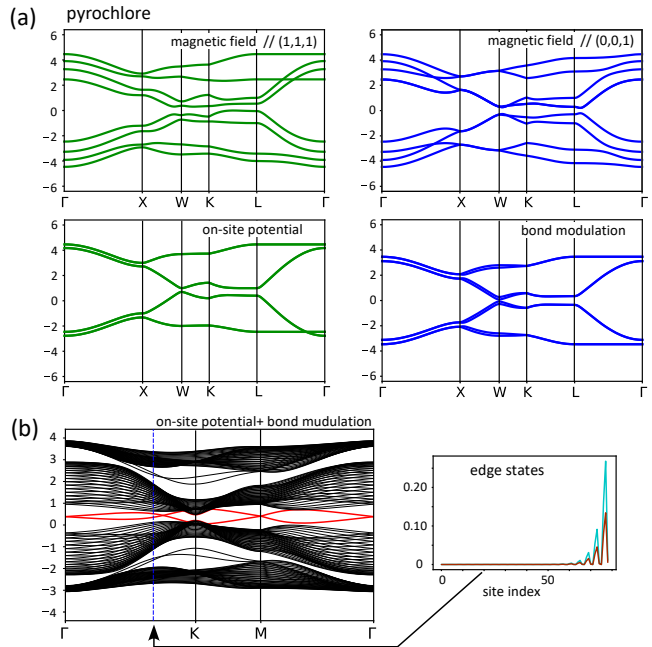


FIG. 3. (a) Band structures of the pyrochlore lattices when we add to Eq.(3) the perturbations shown in Table I: magnetic field $h = 1$ in two different directions, on-site potentials with $(w_1, w_2, w_3, w_4) = (1, 1, 1, 0.4)$, bond modulations. Green/blue bands are non-CS/CS. (b) Recalculated bands with on-site potentials and bond modulation, taking the inter-kagome direction an open boundary, where we find an edge state, indicated in red lines since this case corresponds to the strong TI in class AII. Distributions of edge modes (up/down spins for one mode and otherwise for the other mode) in the open directions.

choice of field direction, CS is preserved. This is in contrast to graphene, where the field generally preserves the CS [45, 46]. The on-site potential keeps the TRS but breaks the PHS, and the CS is always broken. The bond modulation breaks the spatial inversion symmetry and the band degeneracy is lifted, but since it breaks neither TRS nor PHS, the CS is preserved. Several examples of band structures under these perturbations are shown in Fig. 3(a). We show in Fig. 3(b) the bands with on-site

potentials and the bond modulation obtained by taking the inter-kagome plane direction an open boundary. The CS state belonged to class DIII transforms to class AII, where the strong TI is expected [47]. Indeed we see a clear indication of the edge modes.

In conclusion, we found a new mechanism for generating a chiral symmetric band structure; the combination of SOC and the non-bipartite lattice structure based on the triangular loop units allows for the up-spin and down-spin subgroups of basis defined for properly chosen local quantization axis to form a fictitious bipartite lattice; when electrons hop to their neighbors they turnover their spin orientations and belong to the other group. Such condition for CS is detected using the gauge invariant Wilson loop operator on a triangle, and the chiral operator is defined as the product of local gauge transformation that flips the spin quantization axis upside-down. Although the magnetic field may seem to easily break the CS because the equivalence of up/down spin groups is lost, it does not. In our SOC-based CS, several different perturbations can transform the system to different classes in the topological table, which can be easily detected using the Wilson loop operator. Our CS can be extended from the doublet to the multiplet-based models, e.g. in the SU(4) model on a triangular lattice [48].

Acknowledgment. This work was supported by a Grant-in-Aid for Transformative Research Areas "The Natural Laws of Extreme Universe— A New Paradigm for Spacetime and Matter from Quantum Information" (No. 21H05191) and JSPS KAKENHI (No.JP17K05533,JP21K03440). M. K. was supported by JSPS Overseas Research Fellowship.

* nakai-hiroki3510@g.ecc.u-tokyo.ac.jp

† chisa@phys.c.u-tokyo.ac.jp

- [1] J. C. Slater, *Symmetry and energy bands in crystals* (Dover Publications, 1972).
- [2] L. Landau, E. Lifshitz, and M. Pitaevskii, *Statistical Physics* (Butterworth-Heinemann, New York, 1999).
- [3] A. P. Schnyder, S. Ryu, A. Furusaki, and A. W. W. Ludwig, Phys. Rev. B **78**, 195125 (2008).
- [4] A. Kitaev, AIP Conf. Proc. **1134**, 22 (2009).
- [5] J. Kruthoff, J. de Boer, J. van Wezel, C. L. Kane, and R.-J. Slager, Phys. Rev. X **7**, 041069 (2017).
- [6] X. Wen and A. Zee, Nucl. Phys. B **316**, 641 (1989).
- [7] W. P. Su, J. R. Schrieffer, and A. J. Heeger, Phys. Rev. Lett. **42**, 1698 (1979).
- [8] W. P. Su, J. R. Schrieffer, and A. J. Heeger, Phys. Rev. B **22**, 2099 (1980).
- [9] S. Ryu and Y. Hatsugai, Phys. Rev. Lett. **89**, 077002 (2002).
- [10] Y. Hatsugai, T. Fukui, and H. Aoki, Eur. Phys. J. Spec. Top. **148**, 133 (2007).
- [11] Y. Hatsugai, Solid State Commun. **149**, 1061 (2009).
- [12] H. Aoki and M. S. Dresselhaus, *Physics of graphene* (Springer Science & Business Media, 2013).
- [13] E. McCann and V. I. Fal'ko, Phys. Rev. Lett. **96**, 086805 (2006).
- [14] M. I. Katsnelson and M. F. Prokhorova, Phys. Rev. B **77**, 205424 (2008).
- [15] M. Koshino, T. Morimoto, and M. Sato, Phys. Rev. B **90**, 115207 (2014).
- [16] R. Gade and F. Wegner, Nucl. Phys. B **360**, 213 (1991).
- [17] T. Kawarabayashi, Y. Hatsugai, T. Morimoto, and H. Aoki, Phys. Rev. B **83**, 153414 (2011).
- [18] B. Li and A. A. Kovalev, Phys. Rev. B **97**, 174413 (2018).
- [19] J. Verbaarschot, Phys. Rev. Lett. **72**, 2531 (1994).
- [20] X.-G. Wen, *Quantum field theory of many-body systems: from the origin of sound to an origin of light and electrons* (OUP Oxford, 2004).
- [21] S. K. Kim and J. Zang, Phys. Rev. B **92**, 205106 (2015).
- [22] M. Kurita, Y. Yamaji, and M. Imada, J. Phys. Soc. Jpn. **80**, 044708 (2011).
- [23] L. Shekhtman, O. Entin-Wohlman, and A. Aharony, Phys. Rev. Lett. **69**, 836 (1992).
- [24] G. Guarnaccia and C. Noce, Phys. Rev. B **86**, 064409 (2012).
- [25] S. Zhu, Y.-Q. Li, and C. D. Batista, Phys. Rev. B **90**, 195107 (2014).
- [26] S.-S. Zhang, H. Ishizuka, H. Zhang, G. B. Halász, and C. D. Batista, Phys. Rev. B **101**, 024420 (2020).
- [27] B. J. Kim, H. Jin, S. J. Moon, J.-Y. Kim, B.-G. Park, C. S. Leem, J. Yu, T. W. Noh, C. Kim, S.-J. Oh, J.-H. Park, V. Durairaj, G. Cao, and E. Rotenberg, Phys. Rev. Lett. **101**, 076402 (2008).
- [28] D. Uematsu, H. Sagayama, T.-h. Arima, J. J. Ishikawa, S. Nakatsuji, H. Takagi, M. Yoshida, J. Mizuki, and K. Ishii, Phys. Rev. B **92**, 094405 (2015).
- [29] D. I. Khomskii, K. I. Kugel, A. O. Sboychakov, and S. V. Streltsov, J. Exp. Theor. Phys. **122**, 484 (2016).
- [30] T. Takayama, J. Chaloupka, A. Smerald, G. Khaliullin, and H. Takagi, J. Phys. Soc. Jpn. **90**, 062001 (2021).
- [31] D. Yanagishima and Y. Maeno, J. Phys. Soc. Jpn. **70**, 2880 (2001).
- [32] K. Matsuhira, M. Wakeshima, R. Nakanishi, T. Yamada, A. Nakamura, W. Kawano, S. Takagi, and Y. Hinatsu, J. Phys. Soc. Jpn. **76**, 043706 (2007).
- [33] T. F. Qi, O. B. Korneta, X. Wan, L. E. DeLong, P. Schlottmann, and G. Cao, J. Phys. Condens. Matter **24**, 345601 (2012).
- [34] T. Kondo, M. Nakayama, R. Chen, J. J. Ishikawa, E.-G. Moon, T. Yamamoto, Y. Ota, W. Malaeb, H. Kanai, Y. Nakashima, Y. Ishida, R. Yoshida, H. Yamamoto, M. Matsunami, S. Kimura, N. Inami, K. Ono, H. Kumigashira, S. Nakatsuji, L. Balents, and S. Shin, Nat. Commun. **6**, 10042 (2015).
- [35] A. M. Hallas, A. Sharma, C. Mauws, Q. Chen, H. Zhou, C. Ding, Z. Gong, M. Tachibana, P. Sarte, J. Attfield, G. M. Luke, and C. R. Wiebe, npj Quantum Mater. **4**, 9 (2019).
- [36] J. Yamaura, K. Ohgushi, H. Ohsumi, T. Hasegawa, I. Yamauchi, K. Sugimoto, S. Takeshita, A. Tokuda, M. Takata, M. Udagawa, M. Takigawa, H. Harima, T. Arima, and Z. Hiroi, Phys. Rev. Lett. **108**, 247205 (2012).
- [37] K. Kataoka, D. Hirai, A. Koda, R. Kadono, T. Honda, and Z. Hiroi, J. Phys. Condens. Matter **34**, 135602 (2022).
- [38] Y. Okamoto, H. Amano, N. Katayama, H. Sawa,

- K. Niki, R. Mitoka, H. Harima, T. Hasegawa, N. Ogita, Y. Tanaka, M. Takigawa, Y. Yokoyama, K. Takehana, Y. Imanaka, Y. Nakamura, H. Kishida, and K. Takenaka, *Nat. Commun.* **11**, 3144 (2020).
- [39] H. Nakai and C. Hotta, *Nat. Commun.* **13**, 579 (2022).
- [40] Z. Gao and Z. Lan, *Phys. Rev. B* **102**, 245133 (2020).
- [41] E. I. Rashba, *Sov. Phys. Solid State* **2**, 1224 (1960).
- [42] G. Dresselhaus, *Phys. Rev.* **100**, 580 (1955).
- [43] A. Ramachandran, A. Andreanov, and S. Flach, *Phys. Rev. B* **96**, 161104 (2017).
- [44] K. Asano and C. Hotta, *Phys. Rev. B* **83**, 245125 (2011).
- [45] A. J. M. Giesbers, U. Zeitler, M. I. Katsnelson, L. A. Ponomarenko, T. M. Mohiuddin, and J. C. Maan, *Phys. Rev. Lett.* **99**, 206803 (2007).
- [46] Y. Hatsugai, T. Kawarabayashi, and H. Aoki, *Phys. Rev. B* **91**, 085112 (2015).
- [47] W. Witczak-Krempa, A. Go, and Y. B. Kim, *Phys. Rev. B* **87**, 155101 (2013).
- [48] M. G. Yamada, M. Oshikawa, and G. Jackeli, *Phys. Rev. B* **104**, 224436 (2021).

Supplementary material for “Emergent chiral symmetry in non-bipartite kagome and pyrochlore lattices with spin-orbit coupling”

Hiroki Nakai,¹ Masataka Kawano,^{1,2} and Chisa Hotta¹

¹*Department of Basic Science, University of Tokyo, Meguro-ku, Tokyo 153-8902, Japan*

²*Department of Physics, Technical University of Munich, 85748 Garching, Germany*

A. Details of the SOC Hamiltonian

We consider the SOC Hamiltonian in Eq.(3) in the main text, and show their explicit forms.

1. kagome lattice

For the kagome lattice, we take the lattice vectors as $\mathbf{a}_1 = (1, 0)$, $\mathbf{a}_2 = \left(\frac{1}{2}, \frac{\sqrt{3}}{2}\right)$, and coordinates of three sublattices in the unit cell as $\mathbf{r}_1 = (0, 0)$, $\mathbf{r}_2 = \left(\frac{1}{4}, \frac{\sqrt{3}}{4}\right)$ and $\mathbf{r}_3 = \left(\frac{1}{2}, 0\right)$ (Fig.S1 (a)). In the corresponding first Brillouin zone in reciprocal space, the highly symmetric points are defined as $\Gamma = (0, 0)$, $K = \left(\frac{4\pi}{3}, 0\right)$, and $M = \left(\pi, \frac{\pi}{\sqrt{3}}\right)$.

The rotational axes of SU(2) gauge field in the Hamiltonian Eq.(3) for the kagome lattice using the above coordinates are given as, $\hat{\nu}_{12} = (0, 0, -1)$, $\hat{\nu}_{13} = (0, 0, 1)$, and $\hat{\nu}_{23} = (0, 0, -1)$. By constructing the basis in the order $(c_{\mathbf{k}1\uparrow}^\dagger, c_{\mathbf{k}1\downarrow}^\dagger, c_{\mathbf{k}2\uparrow}^\dagger, c_{\mathbf{k}2\downarrow}^\dagger, c_{\mathbf{k}3\uparrow}^\dagger, c_{\mathbf{k}3\downarrow}^\dagger)$, for $\mathcal{H} = \sum_{\mathbf{k}} \mathbf{c}_{\mathbf{k}}^\dagger \mathcal{H}(\mathbf{k}) \mathbf{c}_{\mathbf{k}}$, the Bloch Hamiltonian is obtained in the 6×6 form;

$$\mathcal{H}(\mathbf{k}) = \begin{pmatrix} 0 & h_{12}(\mathbf{k}) & h_{13}(\mathbf{k}) \\ h_{21}(\mathbf{k}) & 0 & h_{23}(\mathbf{k}) \\ h_{31}(\mathbf{k}) & h_{32}(\mathbf{k}) & 0 \end{pmatrix}, \quad (\text{S1})$$

where $h_{ij}(\mathbf{k}) = -2tU_{ij} \cos(\mathbf{k} \cdot (\mathbf{r}_i - \mathbf{r}_j))$.

2. pyrochlore lattice

We consider four sites in a unit cell with the lattice vectors given as $\mathbf{a}_1 = \left(\frac{1}{2}, -\frac{1}{2}, 0\right)$, $\mathbf{a}_2 = \left(0, -\frac{1}{2}, \frac{1}{2}\right)$, and $\mathbf{a}_3 = \left(\frac{1}{2}, 0, \frac{1}{2}\right)$ (Fig.S1 (b)). The corresponding reciprocal lattice vectors are $\mathbf{b}_1 = 2\pi(1, -1, -1)$, $\mathbf{b}_2 = 2\pi(-1, -1, 1)$, $\mathbf{b}_3 = 2\pi(1, 1, 1)$. The coordinates of four sublattices in the unit cell are given as $\mathbf{r}_1 = \left(\frac{1}{8}, \frac{3}{8}, \frac{1}{8}\right)$, $\mathbf{r}_2 = \left(\frac{3}{8}, \frac{1}{8}, \frac{1}{8}\right)$, $\mathbf{r}_3 = \left(\frac{1}{8}, \frac{1}{8}, \frac{3}{8}\right)$, and $\mathbf{r}_4 = \left(\frac{3}{8}, \frac{3}{8}, \frac{3}{8}\right)$. The highly symmetric points in the 1st Brillouin zone are $X = (0, 0, 2\pi)$, $K = \left(\frac{3\pi}{2}, 0, \frac{3\pi}{2}\right)$, $W = (\pi, 0, 2\pi)$, and $L = (\pi, \pi, \pi)$.

The rotational axes of SU(2) gauge field are taken as $\hat{\nu}_{12} = \left(\frac{1}{\sqrt{2}}, \frac{1}{\sqrt{2}}, 0\right)$, $\hat{\nu}_{13} = \left(0, -\frac{1}{\sqrt{2}}, -\frac{1}{\sqrt{2}}\right)$, $\hat{\nu}_{14} = \left(-\frac{1}{\sqrt{2}}, 0, \frac{1}{\sqrt{2}}\right)$, $\hat{\nu}_{23} = \left(\frac{1}{\sqrt{2}}, 0, \frac{1}{\sqrt{2}}\right)$, $\hat{\nu}_{24} = \left(0, \frac{1}{\sqrt{2}}, -\frac{1}{\sqrt{2}}\right)$, $\hat{\nu}_{34} = \left(\frac{1}{\sqrt{2}}, -\frac{1}{\sqrt{2}}, 0\right)$, and the representation of the Bloch Hamiltonian for the basis taken in the order,

$(c_{\mathbf{k}1\uparrow}^\dagger, c_{\mathbf{k}1\downarrow}^\dagger, \dots, c_{\mathbf{k}4\uparrow}^\dagger, c_{\mathbf{k}4\downarrow}^\dagger)$, is given as,

$$\mathcal{H}(\mathbf{k}) = \begin{pmatrix} 0 & h_{12}(\mathbf{k}) & h_{13}(\mathbf{k}) & h_{14}(\mathbf{k}) \\ h_{21}(\mathbf{k}) & 0 & h_{23}(\mathbf{k}) & h_{24}(\mathbf{k}) \\ h_{31}(\mathbf{k}) & h_{32}(\mathbf{k}) & 0 & h_{34}(\mathbf{k}) \\ h_{41}(\mathbf{k}) & h_{42}(\mathbf{k}) & h_{43}(\mathbf{k}) & 0 \end{pmatrix}, \quad (\text{S2})$$

where $h_{ij}(\mathbf{k}) = -2tU_{ij} \cos(\mathbf{k} \cdot (\mathbf{r}_i - \mathbf{r}_j))$.

B. Wilson loop operator

The Wilson loop operator is the path-ordered product of SU(2) gauge fields U_{ij} given in the main text as

$$P(C_{i,jk}) = \exp \left[-i \frac{\Phi}{2} \hat{\mathbf{n}}_{i,jk} \cdot \boldsymbol{\sigma} \right]. \quad (4)$$

In this section, we first derive the two gauge invariant properties from this definition. Then, we construct a chiral operator using the properties related to the Wilson loop operator. Finally, we clarify the definition of “Abelian/non-Abelian” used in this paper, which is different from the non-Abelian properties discussed in other works. We show an example that the Wilson loop operator can be used to determine the Abelian/non-Abelian properties.

1. Proof of gauge invariance of Φ and $\hat{\mathbf{n}}_{i,jk} \cdot \hat{\mathbf{n}}_{i,lm}$

We prove that the rotation angle Φ and the relative angle between rotation axes, $\hat{\mathbf{n}}_{i,jk} \cdot \hat{\mathbf{n}}_{i,lm}$, are both gauge invariant. Using the local gauge transformation operator, $V_i = \exp \left[-i \frac{\varphi_i}{2} \hat{\mathbf{m}}_i \cdot \boldsymbol{\sigma} \right]$, the Wilson loop operator is transformed as

$$\begin{aligned} V_i P(C_{i,jk}) V_i^\dagger &= \cos \frac{\Phi}{2} I - i (\hat{\mathbf{n}}_{i,jk} \cdot \boldsymbol{\sigma}) \cos \varphi_i \sin \frac{\Phi}{2} \\ &\quad - i (\hat{\mathbf{m}}_i \times \hat{\mathbf{n}}_{i,jk}) \cdot \boldsymbol{\sigma} \sin \varphi_i \sin \frac{\Phi}{2} \\ &\quad - i (\hat{\mathbf{m}}_i \cdot \hat{\mathbf{n}}_{i,jk}) (\hat{\mathbf{m}}_i \cdot \boldsymbol{\sigma}) (1 - \cos \varphi_i) \sin \frac{\Phi}{2} \\ &= \cos \frac{\Phi}{2} I - i (\hat{\mathbf{n}}'_{i,jk} \cdot \boldsymbol{\sigma}) \sin \frac{\Phi}{2} \\ &= \exp \left[-i \frac{\Phi}{2} \hat{\mathbf{n}}'_{i,jk} \cdot \boldsymbol{\sigma} \right], \end{aligned} \quad (\text{S3})$$

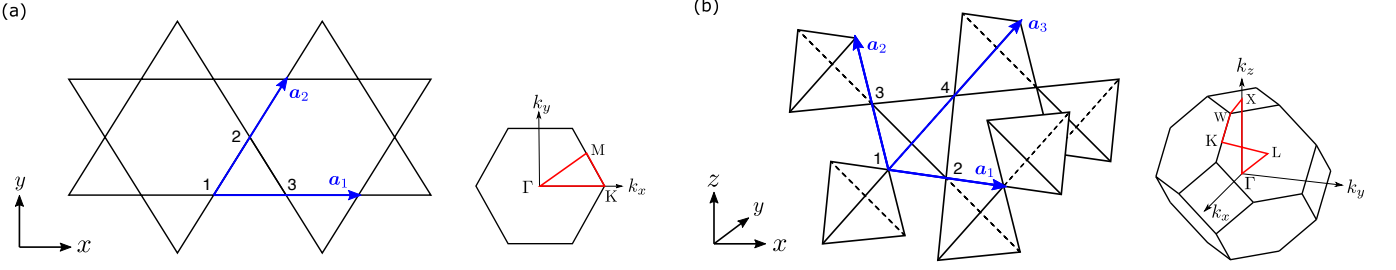


Figure S1. (a) Kagome lattice and (b) pyrochlore lattice. The corresponding Brillouin zone and the representative k -points are shown together.

where

$$\hat{\mathbf{n}}'_{i,jk} = \cos \varphi_i \hat{\mathbf{n}}_{i,jk} + \sin \varphi_i (\hat{\mathbf{m}}_i \times \hat{\mathbf{n}}_{i,jk}) + (1 - \cos \varphi_i) (\hat{\mathbf{m}}_i \cdot \hat{\mathbf{n}}_{i,jk}) \hat{\mathbf{m}}_i. \quad (\text{S4})$$

We immediately see that phase Φ remains unchanged. We now take the inner product between two rotation axes belonging to the same site- i but to different loops, $C_{i,jk} : i \rightarrow j \rightarrow k \rightarrow i$ and $C_{i,lm} : i \rightarrow l \rightarrow m \rightarrow i$, as,

$$\begin{aligned} & \hat{\mathbf{n}}'_{i,jk} \cdot \hat{\mathbf{n}}'_{i,lm} \\ &= \cos^2 \varphi_i \hat{\mathbf{n}}_{i,jk} \cdot \hat{\mathbf{n}}_{i,lm} + \sin \varphi_i \cos \varphi_i (\hat{\mathbf{m}}_i \times \hat{\mathbf{n}}_{i,jk}) \cdot \hat{\mathbf{n}}_{i,lm} \\ & \quad + \cos \varphi_i (1 - \cos \varphi_i) (\hat{\mathbf{m}}_i \cdot \hat{\mathbf{n}}_{i,jk}) (\hat{\mathbf{m}}_i \cdot \hat{\mathbf{n}}_{i,lm}) \\ & \quad + \sin \varphi_i \cos \varphi_i (\hat{\mathbf{m}}_i \times \hat{\mathbf{n}}_{i,lm}) \cdot \hat{\mathbf{n}}_{i,jk} \\ & \quad + \sin^2 \varphi_i (\hat{\mathbf{m}}_i \times \hat{\mathbf{n}}_{i,jk}) \cdot (\hat{\mathbf{m}}_i \times \hat{\mathbf{n}}_{i,lm}) \\ & \quad + \sin \varphi_i (1 - \cos \varphi_i) (\hat{\mathbf{m}}_i \cdot \hat{\mathbf{n}}_{i,jk}) \hat{\mathbf{m}}_i \cdot (\hat{\mathbf{m}}_i \times \hat{\mathbf{n}}_{i,lm}) \\ & \quad + \cos \varphi_i (1 - \cos \varphi_i) (\hat{\mathbf{m}}_i \cdot \hat{\mathbf{n}}_{i,jk}) (\hat{\mathbf{m}}_i \cdot \hat{\mathbf{n}}_{i,lm}) \\ & \quad + \sin \varphi_i (1 - \cos \varphi_i) (\hat{\mathbf{m}}_i \cdot \hat{\mathbf{n}}_{i,lm}) \hat{\mathbf{m}}_i \cdot (\hat{\mathbf{m}}_i \times \hat{\mathbf{n}}_{i,jk}) \\ & \quad + (1 - \cos \varphi_i)^2 (\hat{\mathbf{m}}_i \cdot \hat{\mathbf{n}}_{i,jk}) (\hat{\mathbf{m}}_i \cdot \hat{\mathbf{n}}_{i,lm}). \end{aligned} \quad (\text{S5})$$

The second and fourth terms cancel each other out, and the sixth and eighth terms are zero. Putting together the third, seventh, and ninth terms, we get $(1 - \cos^2 \varphi_i) (\hat{\mathbf{m}}_i \cdot \hat{\mathbf{n}}_{i,jk}) (\hat{\mathbf{m}}_i \cdot \hat{\mathbf{n}}_{i,lm})$. Therefore,

$$\begin{aligned} \hat{\mathbf{n}}'_{i,jk} \cdot \hat{\mathbf{n}}'_{i,lm} &= \cos^2 \varphi_i \hat{\mathbf{n}}_{i,jk} \cdot \hat{\mathbf{n}}_{i,lm} \\ & \quad + (1 - \cos^2 \varphi_i) (\hat{\mathbf{m}}_i \cdot \hat{\mathbf{n}}_{i,jk}) (\hat{\mathbf{m}}_i \cdot \hat{\mathbf{n}}_{i,lm}) \\ & \quad + \sin^2 \varphi_i (\hat{\mathbf{m}}_i \times \hat{\mathbf{n}}_{i,jk}) \cdot (\hat{\mathbf{m}}_i \times \hat{\mathbf{n}}_{i,lm}), \end{aligned} \quad (\text{S6})$$

and

$$\begin{aligned} & (\hat{\mathbf{m}}_i \times \hat{\mathbf{n}}_{i,jk}) \cdot (\hat{\mathbf{m}}_i \times \hat{\mathbf{n}}_{i,lm}) \\ &= (\hat{\mathbf{m}}_i \cdot \hat{\mathbf{m}}_i) (\hat{\mathbf{n}}_{i,jk} \cdot \hat{\mathbf{n}}_{i,lm}) - (\hat{\mathbf{m}}_i \cdot \hat{\mathbf{n}}_{i,jk}) (\hat{\mathbf{m}}_i \cdot \hat{\mathbf{n}}_{i,lm}) \\ &= \hat{\mathbf{n}}_{i,jk} \cdot \hat{\mathbf{n}}_{i,lm} - (\hat{\mathbf{m}}_i \cdot \hat{\mathbf{n}}_{i,jk}) (\hat{\mathbf{m}}_i \cdot \hat{\mathbf{n}}_{i,lm}), \end{aligned} \quad (\text{S7})$$

and we obtain

$$\hat{\mathbf{n}}'_{i,jk} \cdot \hat{\mathbf{n}}'_{i,lm} = \hat{\mathbf{n}}_{i,jk} \cdot \hat{\mathbf{n}}_{i,lm}. \quad (\text{S8})$$

2. How to construct a chiral operator

Let us explain how to construct the chiral operator when (i) $\Phi = \pi$ and (ii) $\{\hat{\mathbf{n}}_{i,jk}\}_i$ is collinear or coplanar. First of all, for rotation axes satisfying (ii), we can take a unit vector $\hat{\mathbf{m}}_i$, which is perpendicular to all $\{\hat{\mathbf{n}}_{i,jk}\}_i$ that belong to site- i . Then, we find $V_i = \exp[-i\frac{\pi}{2} \hat{\mathbf{m}}_i \cdot \boldsymbol{\sigma}] = -i\hat{\mathbf{m}}_i \cdot \boldsymbol{\sigma}$. Since $\hat{\mathbf{m}}_i \cdot \hat{\mathbf{n}}_{i,jk} = 0$,

$$\begin{aligned} V_i P(C_{i,jk}) V_i^\dagger &= (-i\hat{\mathbf{m}}_i \cdot \boldsymbol{\sigma}) (-i\hat{\mathbf{n}}_{i,jk} \cdot \boldsymbol{\sigma}) (i\hat{\mathbf{m}}_i \cdot \boldsymbol{\sigma}) \\ &= +i\hat{\mathbf{n}}_{i,jk} \cdot \boldsymbol{\sigma} = -P(C_{i,jk}). \end{aligned} \quad (\text{S9})$$

Next, to consistently generate the nearby V_j ($j \neq i$) from V_i , the form

$$V_j = U_{jk} U_{ki} V_i U_{ik} U_{kj}, \quad k \neq i, j, \quad (\text{S10})$$

gives the natural extension using the SU(2) gauge. This form immediately gives $V_i U_{ij} V_j^\dagger = -U_{ij}$, $\forall i, j$ e.g.,

$$\begin{aligned} V_i U_{ij} V_j^\dagger &= V_i U_{ij} U_{jk} U_{ki} V_i^\dagger U_{ik} U_{kj} \\ &= V_i P(C_{i,kj}) V_i^\dagger U_{ik} U_{kj} \\ &= -P(C_{i,kj}) U_{ik} U_{kj} \\ &= -U_{ij} U_{jk} U_{ki} U_{ik} U_{kj} \\ &= -U_{ij}, \end{aligned} \quad (\text{S11})$$

and

$$\begin{aligned} V_l U_{lj} V_j^\dagger &= U_{lm} U_{mi} V_i U_{im} U_{ml} U_{lj} U_{jk} U_{ki} V_i^\dagger U_{ik} U_{kj} \\ &= U_{lj} U_{ji} V_i P(C_{i,kj}) V_i^\dagger U_{ik} U_{kj} \\ &= -U_{lj} U_{ji} P(C_{i,kj}) U_{ik} U_{kj} \\ &= -U_{lj} U_{ji} U_{ij} U_{jk} U_{ki} U_{ik} U_{kj} \\ &= -U_{lj}. \end{aligned} \quad (\text{S12})$$

In the second example, there appears a product of SU(2) gauge fields, $U_{im} U_{ml} U_{lj} U_{jk} U_{ki}$, along the path $i \rightarrow k \rightarrow j \rightarrow l \rightarrow m \rightarrow i$. Since the loops defined on the pyrochlore and triangular lattice cannot return to the original site by five independent bonds, two of the five bonds should be the same ones, which we chose as j - l and l - m , i.e. $U_{ml} U_{lj} = 1$.

We show another construction of the chiral operator, applied to a more general case including the parameter

region off the chiral symmetric points. We take $\hat{\mathbf{r}}_{Ci}$ as a unit vector that points from site- i to the center of triangle or tetrahedron C . When $V_i = \exp[-i\frac{\pi}{2}\hat{\mathbf{r}}_{Ci} \cdot \boldsymbol{\sigma}]$,

$$V_i U_{ij}(\theta) V_j^\dagger = -U_{ij}(\alpha - \theta \pm 2\pi), \quad (\text{S13})$$

where α satisfy $\hat{\mathbf{r}}_{Ci} \cdot \hat{\mathbf{r}}_{Cj} = \cos(\alpha/2)$, $\hat{\mathbf{r}}_{Ci} \times \hat{\mathbf{r}}_{Cj} = -\sin(\alpha/2)\hat{\nu}_{ij}$, and $0 < \alpha < 2\pi$. Because the unitary operator $\tilde{\Gamma} = \oplus_{j=1}^n iV_j$ satisfy

$$\tilde{\Gamma} \mathcal{H}(\mathbf{k}, \theta) \tilde{\Gamma}^\dagger = -\mathcal{H}(\mathbf{k}, \alpha - \theta \pm 2\pi), \quad (\text{S14})$$

the energy eigenvalues of $\mathcal{H}(\mathbf{k}, \theta)$ have opposite sign and the same amplitude as those of $\mathcal{H}(\mathbf{k}, \alpha - \theta \pm 2\pi)$. Since the top bands are flat at $\theta = 0$, flat bands appear at the bottom when $\theta = \alpha \pm 2\pi$. If there exists θ_0 that fulfills $\theta_0 = \alpha - \theta_0 \pm 2\pi$, $\mathcal{H}(\mathbf{k}, \theta_0)$ has a chiral symmetry; it corresponds to $\theta_0 = \arccos(-1/2) - \pi$ for kagome lattice, and $\theta_0 = \arccos(-1/3) - \pi$ for pyrochlore lattice. In addition to that, since θ_0 satisfies

$$\Phi(\theta_0 + \varphi) = 2\pi - \Phi(\theta_0 - \varphi) \quad (\text{S15})$$

for arbitrary φ , then $\Phi(\theta)$ is symmetric about $(\theta, \Phi) = (\theta_0, \pi)$.

3. Abelian and non-Abelian gauge fields

We use the terminology, ‘‘Abelian/non-Abelian’’ according to whether or not there exists a gauge that makes the SU(2) gauge fields U_{ij} defined on different bonds commutative. This definition is more rigorous than the ones used in the previous articles; in general, when the SU(2) gauge field appears in the Hamiltonian, they simply call it ‘‘non-Abelian’’¹, but it can become Abelian with the aid of spatial symmetry, e.g. the site-centered inversion symmetry of a kagome lattice gives rise to the U(1) symmetry². However, even if U_{ij} is ‘‘non-Abelian’’, namely noncommutative *in some certain choices of the gauge*, if there is at least one way of taking the gauge that makes U_{ij} commutative, the features linked to the non-commutativity do not appear in gauge-invariant physical quantities such as band structure or topological numbers. Since we are interested in the properties related to the non-commutativity of the gauge field, these properties can in turn enable us to judge whether the gauge is non-Abelian or not.

Let us show here that Φ is such property; If the gauge field is Abelian in our sense, one can simultaneously invert the rotation axis $\hat{\nu}_{ij}$ of all U_{ij} by a local gauge transformation, which is equivalent to taking $\theta \rightarrow -\theta$. Then, since Φ is a gauge invariant quantity, one can say that if the gauge field is Abelian, $\Phi(\theta) = \Phi(-\theta)$ should hold. Conversely, if $\Phi(\theta) \neq \Phi(-\theta)$, the gauge field is non-Abelian. This condition works in Fig. 1(e) in the main text to find immediately that the SU(2) gauge field of the pyrochlore lattice is non-Abelian since $\Phi(\theta) \neq \Phi(-\theta)$.

C. Symmetry analysis

In this section, we clarify several aspects of underlying symmetries of the energy eigenstates at chiral symmetric points. First, we show that the U(1) symmetry in spin space allows us to block-diagonalize the Bloch Hamiltonian when it is collinear ($\theta = \theta_1$ in the kagome lattice and θ_2 in the pyrochlore lattice), and that the diagonal block is described by a sublattice pseudospin due to chiral symmetry. Partially making use of the sublattice pseudospin picture, we next show that the chiral zero modes in the pyrochlore lattice are protected by the chiral symmetry and the spatial symmetry and appear at a specific point or line in momentum space, where the bands become degenerate.

1. sublattice pseudospin

Let us consider the collinear case, i.e., when the Wilson loop operators starting from site- i represent the rotation around the same axis independent of their paths. Note that the rotation axis $\hat{\mathbf{n}}_{i,jk}$ is different at the different base site i . Considering the local gauge transformation V_i represented by the rotation around its axis, we find that $V = \oplus_{i=1}^n V_i$ is commutative with the Bloch Hamiltonian. It is confirmed in the same way as when we construct the chiral operator. In the basis that diagonalizes V , the sublattices $i = 1, 2, \dots, n$ remain unchanged from the original basis. The Bloch Hamiltonian $\mathcal{H}(\mathbf{k})$ is therefore block-diagonalized and expressed as $\text{diag}(D(\mathbf{k}), D^*(\mathbf{k}))$ due to time reversal symmetry and site-centered inversion symmetry; $D(\mathbf{k})$ is a $n \times n$ Hermitian matrix, and serves as a Hamiltonian about the sublattice degrees of freedom. We investigate the constraints on $D(\mathbf{k})$ imposed by the chiral symmetry for the kagome lattice ($n = 3$) and for the pyrochlore lattice ($n = 4$).

We first consider the kagome lattice, whose $D(\mathbf{k})$ is expanded as

$$D(\mathbf{k}) = \sum_{i=1}^8 R_i(\mathbf{k})\tau_i, \quad (\text{S16})$$

where $(\tau_1, \tau_2, \dots, \tau_8)$ are Gell-Mann matrices:

$$\begin{aligned} \tau_1 &= \begin{pmatrix} 0 & 1 & 0 \\ 1 & 0 & 0 \\ 0 & 0 & 0 \end{pmatrix}, & \tau_2 &= \begin{pmatrix} 0 & -i & 0 \\ i & 0 & 0 \\ 0 & 0 & 0 \end{pmatrix}, & \tau_3 &= \begin{pmatrix} 1 & 0 & 0 \\ 0 & -1 & 0 \\ 0 & 0 & 0 \end{pmatrix}, \\ \tau_4 &= \begin{pmatrix} 0 & 0 & 1 \\ 0 & 0 & 0 \\ 1 & 0 & 0 \end{pmatrix}, & \tau_5 &= \begin{pmatrix} 0 & 0 & -i \\ 0 & 0 & 0 \\ i & 0 & 0 \end{pmatrix}, & \tau_6 &= \begin{pmatrix} 0 & 0 & 0 \\ 0 & 0 & 1 \\ 0 & 1 & 0 \end{pmatrix}, \\ \tau_7 &= \begin{pmatrix} 0 & 0 & 0 \\ 0 & 0 & -i \\ 0 & i & 0 \end{pmatrix}, & \tau_8 &= \frac{1}{\sqrt{3}} \begin{pmatrix} 1 & 0 & 0 \\ 0 & 1 & 0 \\ 0 & 0 & -2 \end{pmatrix}. \end{aligned} \quad (\text{S17})$$

Since the electron hops only between different sublattices, diagonal element of $\mathcal{H}(\mathbf{k})$ is zero and $R_3(\mathbf{k}) = R_8(\mathbf{k}) = 0$.

In the above given basis, the chiral operator Γ is expressed as

$$\Gamma = \begin{pmatrix} & \gamma \\ \gamma^* & \end{pmatrix}, \quad \gamma = \text{diag}(z^*, i, -z), \quad z = e^{i\frac{\pi}{6}}. \quad (\text{S18})$$

Since

$$\Gamma \mathcal{H}(\mathbf{k}) \Gamma^\dagger = \begin{pmatrix} \gamma D(\mathbf{k}) \gamma^* & \\ & \gamma^* D(\mathbf{k}) \gamma \end{pmatrix}, \quad (\text{S19})$$

the chiral symmetry, $\{\mathcal{H}(\mathbf{k}), \Gamma\} = 0$, requires $\gamma^* D(\mathbf{k}) \gamma = -D^*(\mathbf{k})$. Here,

$$\begin{aligned} \gamma^* \tau_1 \gamma &= -\frac{1}{2} \tau_1 - \frac{\sqrt{3}}{2} \tau_2, & \gamma^* \tau_2 \gamma &= \frac{\sqrt{3}}{2} \tau_1 - \frac{1}{2} \tau_2, \\ \gamma^* \tau_4 \gamma &= -\frac{1}{2} \tau_4 + \frac{\sqrt{3}}{2} \tau_5, & \gamma^* \tau_5 \gamma &= -\frac{\sqrt{3}}{2} \tau_4 - \frac{1}{2} \tau_5, \\ \gamma^* \tau_6 \gamma &= -\frac{1}{2} \tau_6 - \frac{\sqrt{3}}{2} \tau_7, & \gamma^* \tau_7 \gamma &= \frac{\sqrt{3}}{2} \tau_6 - \frac{1}{2} \tau_7, \end{aligned} \quad (\text{S20})$$

and then,

$$\begin{aligned} &\gamma^* D(\mathbf{k}) \gamma \\ &= \left(-\frac{1}{2} R_1(\mathbf{k}) + \frac{\sqrt{3}}{2} R_2(\mathbf{k}) \right) \tau_1 - \left(\frac{\sqrt{3}}{2} R_1(\mathbf{k}) + \frac{1}{2} R_2(\mathbf{k}) \right) \tau_2 \\ &\quad - \left(\frac{1}{2} R_4(\mathbf{k}) + \frac{\sqrt{3}}{2} R_5(\mathbf{k}) \right) \tau_4 + \left(\frac{\sqrt{3}}{2} R_4(\mathbf{k}) - \frac{1}{2} R_5(\mathbf{k}) \right) \tau_5 \\ &\quad - \left(\frac{1}{2} R_6(\mathbf{k}) - \frac{\sqrt{3}}{2} R_7(\mathbf{k}) \right) \tau_6 - \left(\frac{\sqrt{3}}{2} R_6(\mathbf{k}) + \frac{1}{2} R_7(\mathbf{k}) \right) \tau_7. \end{aligned} \quad (\text{S21})$$

On the other hand, since

$$\begin{aligned} -D^*(\mathbf{k}) &= -R_1(\mathbf{k}) \tau_1 + R_2(\mathbf{k}) \tau_2 - R_4(\mathbf{k}) \tau_4 + R_5(\mathbf{k}) \tau_5 \\ &\quad - R_6(\mathbf{k}) \tau_6 + R_7(\mathbf{k}) \tau_7, \end{aligned} \quad (\text{S22})$$

we obtain three constraints

$$\begin{aligned} R_1(\mathbf{k}) + \sqrt{3} R_2(\mathbf{k}) &= 0, & R_4(\mathbf{k}) - \sqrt{3} R_5(\mathbf{k}) &= 0, \\ R_6(\mathbf{k}) + \sqrt{3} R_7(\mathbf{k}) &= 0. \end{aligned} \quad (\text{S23})$$

Using these constraints, we can reduce the number of basis to three, and by defining $\tilde{\mathbf{R}}(\mathbf{k})$ and \mathbf{S} as

$$\begin{aligned} \tilde{R}_1(\mathbf{k}) &= \frac{\sqrt{3}}{2} R_6(\mathbf{k}) - \frac{1}{2} R_7(\mathbf{k}), \\ \tilde{R}_2(\mathbf{k}) &= \frac{\sqrt{3}}{2} R_4(\mathbf{k}) + \frac{1}{2} R_5(\mathbf{k}), \\ \tilde{R}_3(\mathbf{k}) &= \frac{\sqrt{3}}{2} R_1(\mathbf{k}) - \frac{1}{2} R_2(\mathbf{k}), \end{aligned} \quad (\text{S24})$$

$$\begin{aligned} S_x &= \frac{\sqrt{3}}{2} \tau_6 - \frac{1}{2} \tau_7 = \begin{pmatrix} 0 & 0 & 0 \\ 0 & 0 & z \\ 0 & z^* & 0 \end{pmatrix}, \\ S_y &= \frac{\sqrt{3}}{2} \tau_4 + \frac{1}{2} \tau_5 = \begin{pmatrix} 0 & 0 & z^* \\ 0 & 0 & 0 \\ z & 0 & 0 \end{pmatrix}, \\ S_z &= \frac{\sqrt{3}}{2} \tau_1 - \frac{1}{2} \tau_2 = \begin{pmatrix} 0 & z & 0 \\ z^* & 0 & 0 \\ 0 & 0 & 0 \end{pmatrix}, \end{aligned} \quad (\text{S25})$$

$D(\mathbf{k})$ is expressed as

$$D(\mathbf{k}) = \sum_{i=1}^3 \tilde{R}_i(\mathbf{k}) S_i. \quad (\text{S26})$$

From Eq.(S25), we find that \mathbf{S} fulfills the commutation relation,

$$[S_i, S_j] = i \varepsilon_{ijk} S_k, \quad \mathbf{S}^2 = 2I, \quad (\text{S27})$$

meaning that \mathbf{S} serves as a pseudospin-1 operator of the sublattice degrees of freedom.

Next, we consider the pyrochlore lattice. In general, the Bloch Hamiltonian for pyrochlore lattice cannot be block-diagonalized because of its non-Abelian property. However, at $\theta = \theta_2 = 2 \arctan(\sqrt{2})$, which is the collinear case, the system recovers the Abelian property and $\mathcal{H}(\mathbf{k})$ can be block-diagonalized into $\text{diag}(D(\mathbf{k}), D^*(\mathbf{k}))$. Here, $D(\mathbf{k})$ is expanded as

$$D(\mathbf{k}) = \sum_{i=1}^{15} R_i(\mathbf{k}) \Omega_i, \quad (\text{S28})$$

where $(\Omega_1, \Omega_2, \dots, \Omega_{15})$ are linearly independent traceless matrices:

$$\begin{aligned} \Omega_1 &= \sigma_0 \otimes \sigma_x, & \Omega_2 &= \sigma_0 \otimes \sigma_y, & \Omega_3 &= \sigma_0 \otimes \sigma_z, \\ \Omega_4 &= \sigma_x \otimes \sigma_x, & \Omega_5 &= \sigma_x \otimes \sigma_y, & \Omega_6 &= \sigma_x \otimes \sigma_z, \\ \Omega_7 &= \sigma_y \otimes \sigma_x, & \Omega_8 &= \sigma_y \otimes \sigma_y, & \Omega_9 &= \sigma_y \otimes \sigma_z, \\ \Omega_{10} &= \sigma_z \otimes \sigma_x, & \Omega_{11} &= \sigma_z \otimes \sigma_y, & \Omega_{12} &= \sigma_z \otimes \sigma_z, \\ \Omega_{13} &= \sigma_x \otimes \sigma_0, & \Omega_{14} &= \sigma_y \otimes \sigma_0, & \Omega_{15} &= \sigma_z \otimes \sigma_0. \end{aligned} \quad (\text{S29})$$

As in the case of the kagome lattice, we set the coefficients as $R_7(\mathbf{k}) = R_{12}(\mathbf{k}) = R_{14}(\mathbf{k}) = 0$, whose corresponding Ω_i have diagonal elements. The chiral operator is expressed as

$$\Gamma = \begin{pmatrix} & \gamma \\ \gamma^* & \end{pmatrix}, \quad \gamma = \text{diag}(z^{10}, z^{10}, z^4, z^4), \quad z = e^{i\frac{\pi}{6}}. \quad (\text{S30})$$

The constraints arising from the chiral symmetry are derived in the same way as we did for the kagome lattice, and we find that

$$\gamma^* \Omega_i \gamma = \begin{cases} +\Omega_i & i = 1, 2, 10, 11 \\ -\Omega_i & i = 4, 5, 6, 7, 8, 9, 13, 14, \end{cases} \quad (\text{S31})$$

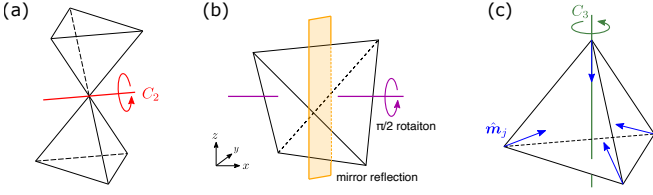


Figure S 2. The symmetry operations. (a) C_2 is a two-fold rotation, which interchange the upward and downward tetrahedra. (b) $s_{4\mu}$ ($\mu = x, y, z$) is a roto-reflection which is a combination of a $\pi/2$ -rotation around the axis parallel to the μ -axis through the center of the tetrahedron, and a mirror reflection across the plane perpendicular to that axis. (c) C_3 is a three-fold rotation, which fix one vertex of the tetrahedron and replace the other three vertices. The quantization axes $\hat{\mathbf{m}}_j$, which diagonalize the chiral operator, are invariant under this rotation.

and from $\gamma^* D(\mathbf{k}) \gamma = -D^*(\mathbf{k})$, we obtain

$$\begin{aligned} R_1(\mathbf{k}) &= R_5(\mathbf{k}) = R_7(\mathbf{k}) = R_9(\mathbf{k}) = R_{10}(\mathbf{k}) = R_{14}(\mathbf{k}) = 0, \\ \mathbf{S}_1 &= (S_{1,x}, S_{1,y}, S_{1,z}) = (-\Omega_2, -\Omega_6, \Omega_4)/2, \\ \mathbf{S}_2 &= (S_{2,x}, S_{2,y}, S_{2,z}) = (-\Omega_{11}, -\Omega_{13}, \Omega_8)/2, \end{aligned} \quad (\text{S32})$$

where \mathbf{S}_1 and \mathbf{S}_2 are the pseudospin- $\frac{1}{2}$ operators, which satisfy,

$$[S_{a,i}, S_{b,j}] = i\delta_{ab}\varepsilon_{ijk}S_{a,k}, \quad \mathbf{S}_a^2 = \frac{3}{4}I. \quad (\text{S33})$$

2. chiral zero modes

We show the existence of the chiral zero modes protected by the chiral symmetry and the spatial symmetry. First, let us discuss the point contact at L and W points at $\theta = \theta_2 = 2\arctan(\sqrt{2})$. As discussed above, the Bloch Hamiltonian is block-diagonalized into $\text{diag}(D(\mathbf{k}), D^*(\mathbf{k}))$ and is expanded as

$$\begin{aligned} D(\mathbf{k}) &= R_2(\mathbf{k})\Omega_2 + R_4(\mathbf{k})\Omega_4 + R_6(\mathbf{k})\Omega_6 \\ &+ R_8(\mathbf{k})\Omega_8 + R_{11}(\mathbf{k})\Omega_{11} + R_{13}(\mathbf{k})\Omega_{13}. \end{aligned} \quad (\text{S34})$$

We now analyze the symmetry of the pyrochlore lattice. Let us set the axis perpendicular to the direction connecting one of the vertices and the center of the tetrahedron. This axis is parallel to one of the edges of the triangle formed by the rest of the vertices. The pyrochlore lattice is invariant under the π -rotations (C_2) about that axis (Fig.S2 (a)). The matrix representation of this operation

for the basis that block-diagonalizes $\mathcal{H}(\mathbf{k})$ is

$$\begin{aligned} C_2 &= \begin{pmatrix} & \tilde{C}_{2,1} \\ \tilde{C}_{2,2} & \end{pmatrix}, \\ \tilde{C}_{2,1} &= \begin{pmatrix} e^{\pi i/3} & & \\ & e^{5\pi i/6} & \\ & & e^{4\pi i/3} \end{pmatrix}, \\ \tilde{C}_{2,2} &= \begin{pmatrix} e^{2\pi i/3} & & \\ & e^{\pi i/6} & \\ & & e^{5\pi i/3} \end{pmatrix}. \end{aligned} \quad (\text{S35})$$

Now, the L points in momentum space are invariant under C_2 , and the Bloch Hamiltonian $\mathcal{H}(\mathbf{k})$ commutes with C_2 as,

$$\begin{aligned} \mathcal{H}(\mathbf{k}) &= C_2 \mathcal{H}(\mathbf{k}) C_2^\dagger \\ &= \begin{pmatrix} & \tilde{C}_{2,1} \\ \tilde{C}_{2,2} & \end{pmatrix} \begin{pmatrix} D(\mathbf{k}) & \\ & D^*(\mathbf{k}) \end{pmatrix} \begin{pmatrix} \tilde{C}_{2,1}^\dagger & \\ & \tilde{C}_{2,2}^\dagger \end{pmatrix} \\ &= \begin{pmatrix} \tilde{C}_{2,1} D^*(\mathbf{k}) \tilde{C}_{2,1}^\dagger & \\ & \tilde{C}_{2,2} D(\mathbf{k}) \tilde{C}_{2,2}^\dagger \end{pmatrix}. \end{aligned} \quad (\text{S36})$$

Then, we find

$$D(\mathbf{k}) = \tilde{C}_{2,1} D^*(\mathbf{k}) \tilde{C}_{2,1}^\dagger, \quad D^*(\mathbf{k}) = \tilde{C}_{2,2} D(\mathbf{k}) \tilde{C}_{2,2}^\dagger, \quad (\text{S37})$$

which lead to

$$\begin{aligned} \tilde{C}_{2,1} \Omega_2^* \tilde{C}_{2,1}^\dagger &= \Omega_{13}, & \tilde{C}_{2,1} \Omega_{13}^* \tilde{C}_{2,1}^\dagger &= \Omega_2, \\ \tilde{C}_{2,1} \Omega_4^* \tilde{C}_{2,1}^\dagger &= \Omega_8, & \tilde{C}_{2,1} \Omega_8^* \tilde{C}_{2,1}^\dagger &= \Omega_4, \\ \tilde{C}_{2,1} \Omega_6^* \tilde{C}_{2,1}^\dagger &= \Omega_{11}, & \tilde{C}_{2,1} \Omega_{11}^* \tilde{C}_{2,1}^\dagger &= \Omega_6. \end{aligned} \quad (\text{S38})$$

We thus find, $R_2(\mathbf{k}) = R_{13}(\mathbf{k})$, $R_4(\mathbf{k}) = R_8(\mathbf{k})$ and $R_6(\mathbf{k}) = R_{11}(\mathbf{k})$.

The same analysis is performed for the other C_2 axes, and we obtain $R_2(\mathbf{k}) = -R_4(\mathbf{k}) = R_6(\mathbf{k}) = -R_8(\mathbf{k}) = R_{11}(\mathbf{k}) = R_{13}(\mathbf{k}) (\equiv R(\mathbf{k}))$. From these relationships, the block-diagonal Hamiltonian at L points is given as

$$\begin{aligned} D(\mathbf{k}) &= R(\mathbf{k})(\Omega_2 - \Omega_4 + \Omega_6 - \Omega_8 + \Omega_{11} + \Omega_{13}) \\ &= -2\mathbf{R}(\mathbf{k}) \cdot (\mathbf{S}_1 + \mathbf{S}_2), \end{aligned} \quad (\text{S39})$$

where $\mathbf{R}(\mathbf{k}) = R(\mathbf{k})(1, 1, 1)$, and its eigenvalues are $\pm 2|\mathbf{R}(\mathbf{k})|$, 0 (doubly degenerate).

The next symmetry operation we consider is the roto-reflection ($s_{4\mu}$ ($\mu = x, y, z$)), the $\pi/2$ -rotation about the axis parallel to the μ -axis through the center of the tetrahedron combined with the mirror operation about the plane perpendicular to that axis (Fig.S2 (b)). Let us

consider $\mu = x$ and this operation is represented by

$$\begin{aligned} s_{4x} &= \begin{pmatrix} & \tilde{s}_{4x,1} \\ \tilde{s}_{4x,2} & \end{pmatrix}, \\ \tilde{s}_{4x,1} &= \begin{pmatrix} & e^{23\pi i/12} & & \\ & & e^{17\pi i/12} & \\ e^{17\pi i/12} & & & e^{11\pi i/12} \end{pmatrix}, \\ \tilde{s}_{4x,2} &= \begin{pmatrix} & e^{19\pi i/12} & & \\ & & e^{\pi i/12} & \\ e^{\pi i/12} & & & e^{7\pi i/12} \end{pmatrix}. \end{aligned} \quad (\text{S40})$$

Now, the W points in momentum space are invariant under this operation and, similar to the above discussion at L points, we find

$$D(\mathbf{k}) = \tilde{s}_{4x,1} D^*(\mathbf{k}) \tilde{s}_{4x,1}^\dagger, \quad D^*(\mathbf{k}) = \tilde{s}_{4x,2} D(\mathbf{k}) \tilde{s}_{4x,2}^\dagger, \quad (\text{S41})$$

which lead to

$$\begin{aligned} \tilde{s}_{4x,1} \Omega_2^* \tilde{s}_{4x,1}^\dagger &= -\Omega_8, & \tilde{s}_{4x,1} \Omega_8^* \tilde{s}_{4x,1}^\dagger &= -\Omega_2, \\ \tilde{s}_{4x,1} \Omega_4^* \tilde{s}_{4x,1}^\dagger &= -\Omega_{11}, & \tilde{s}_{4x,1} \Omega_{11}^* \tilde{s}_{4x,1}^\dagger &= \Omega_4, \\ \tilde{s}_{4x,1} \Omega_6^* \tilde{s}_{4x,1}^\dagger &= \Omega_{13}, & \tilde{s}_{4x,1} \Omega_{13}^* \tilde{s}_{4x,1}^\dagger &= -\Omega_6. \end{aligned} \quad (\text{S42})$$

We thus find, $R_2(\mathbf{k}) = -R_8(\mathbf{k}) (\equiv R(\mathbf{k}))$, $R_4(\mathbf{k}) = R_6(\mathbf{k}) = R_{11}(\mathbf{k}) = R_{13}(\mathbf{k}) = 0$. From these relationships, the block-diagonal Hamiltonian at W points is given as

$$D(\mathbf{k}) = R(\mathbf{k})(\Omega_2 - \Omega_8) = -2R(\mathbf{k})(S_{1,x} + S_{2,z}). \quad (\text{S43})$$

Since $[S_{1,x}, S_{2,z}] = 0$, its eigenvalues are $\pm 2|R(\mathbf{k})|$, 0 (doubly degenerate).

Finally, we consider the nodal Γ - L line at $\theta = \theta_3 = -2 \arctan(1/\sqrt{2})$. Since it is the coplanar case, the block-diagonalization of $\mathcal{H}(\mathbf{k})$ is unavailable, but by combining the chiral symmetry and the spatial symmetry, we can show that there is a band touching at zero energy³. Here, we consider the $2\pi/3$ -rotation (C_3) about an axis that connects one vertex and the center of the tetrahedron. The matrix representation of this operation for the original basis is

$$C_3 = \tilde{C}_3 \otimes \begin{pmatrix} & & 1 \\ & & & 1 \\ 1 & & & \\ & & & & 1 \end{pmatrix}, \quad (\text{S44})$$

where $\tilde{C}_3 = \exp[-i\frac{\pi}{3}\hat{\mathbf{n}} \cdot \boldsymbol{\sigma}]$, $\hat{\mathbf{n}} = (1, 1, 1)/\sqrt{3}$. In the basis that diagonalizes the chiral operator Γ , the quantization axis is $\hat{\mathbf{m}}_j$ at site j . At $\theta = -2 \arctan(1/\sqrt{2})$, it points toward the center of the tetrahedron. Therefore, this quantization axis is invariant under the C_3 operation, and C_3 commutes with Γ (Fig.S2 (c)). Since the Γ - L line is invariant under C_3 , $\mathcal{H}(\mathbf{k})$ commutes with C_3 .

Both Γ and $\mathcal{H}(\mathbf{k})$ that commute with C_3 are block-diagonalized into the eigenspace of C_3 with

eigenvalues being -1 , $\omega_1 = e^{\pi i/3}$, $\omega_2 = e^{5\pi i/3}$. They are, $\Gamma = \text{diag}(\Gamma_{-1}, \Gamma_{\omega_1}, \Gamma_{\omega_2})$ and $\mathcal{H}(\mathbf{k}) = \text{diag}(\mathcal{H}_{-1}(\mathbf{k}), \mathcal{H}_{\omega_1}(\mathbf{k}), \mathcal{H}_{\omega_2}(\mathbf{k}))$, which are anticommutative in their respective blocks as

$$\{\Gamma_a, \mathcal{H}_a(\mathbf{k})\} = 0, \quad a = -1, \omega_1, \omega_2. \quad (\text{S45})$$

$\nu_a = \text{Tr} \Gamma_a$ denotes the difference in the number of zero modes, $N_{a,\pm}$, with positive and negative chirality (eigenvalues of Γ_a is ± 1); $\nu_a = N_{a,+} - N_{a,-}$. Since $\nu_{-1} = 0$, $\nu_{\omega_1} = 1$ and $\nu_{\omega_2} = -1$, there are at least two chiral zero modes. Since this argument holds for \mathbf{k} -points on the Γ - L line, we find that a nodal line appears on the Γ - L line and that it is protected by the chiral symmetry and the three-fold rotation symmetry.

D. Details of perturbation Hamiltonian

We have discussed the effect of small perturbation to Eq.(3) in the main text, and summarized the results in Fig.3 and Table I. We explain the details of these perturbations.

1. uniform magnetic field

We take account of the uniform magnetic field as a Zeeman effect as

$$\mathcal{H}_{\text{mf}} = - \sum_j \mathbf{h} \cdot \mathbf{s}_j, \quad (\text{S46})$$

where $s_{j,\mu} = \mathbf{c}_j^\dagger (\sigma_\mu/2) \mathbf{c}_j$ ($\mu = x, y, z$) is an electron spin operator at site- j . This magnetic field breaks both TRS and PHS, but may or may not break CS. We express the Zeeman term at site- j as $-\mathbf{h} \cdot \boldsymbol{\sigma} = -i \exp[-i\frac{\pi}{2}\mathbf{h} \cdot \boldsymbol{\sigma}]$, and if \mathbf{h} is perpendicular to the quantization axis $\hat{\mathbf{m}}_j$ diagonalizing the chiral operator, then $V_j(-\mathbf{h} \cdot \boldsymbol{\sigma}_j) V_j^\dagger = +\mathbf{h} \cdot \boldsymbol{\sigma}$ holds. When $\mathbf{h} \cdot \hat{\mathbf{m}}_j = 0$ for each site, TRS and PHS are violated, but CS is preserved.

2. on-site potential

We set different values of on-site potentials for n -independent sites in the unit cell

$$\mathcal{H}_{\text{op}} = \sum_{l=1}^n \sum_{j \in l} \omega_l n_j, \quad (\text{S47})$$

where $n_j = \mathbf{c}_j^\dagger \mathbf{c}_j$ is an electron number operator at site j . This on-site potential breaks the PHS but not the TRS, and thus the CS is lost. This can also be interpreted as follows: the term at site- j is expressed as $\omega_j I$, and then this term is shown to be invariant under the local gauge transformation as $V_j(\omega_j I) V_j^\dagger = \omega_j I \neq -\omega_j I$.

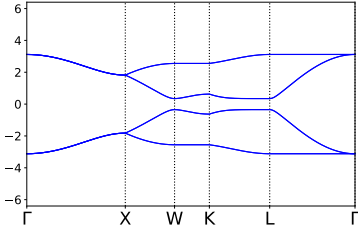


Figure S 3. The band structure at θ_2 for the pyrochlore lattice when bond modulation is $\delta_{ij} = 1$ for all downward tetrahedra. The band degeneracy is not lifted even though the spatial inversion symmetry is broken.

3. bond modulation

The effect of bond modulation influences the hopping amplitude t_0, λ in a nontrivial manner, because the crys-

tal field is varied. However, for simplicity, we consider the simplest modulation called breathing: among the two types of tetrahedra pointing up and down, only one of them is subject to the modulation as $t_{ij}^{\text{up}} = t$, $t_{ij}^{\text{down}} = \delta_{ij}t$. This does not modify the $SU(2)$ gauge field U_{ij} , which preserves the chiral symmetry. Moreover, since the TRS is not broken, the PHS is also preserved, and the class to which the Bloch Hamiltonian belongs remains unchanged.

This bond modulation breaks the spatial inversion symmetry of the lattice, which lifts the band-degeneracy in general. When $\delta_{12} = \delta_{34}$, $\delta_{13} = \delta_{24}$ and $\delta_{14} = \delta_{23}$, even though the space inversion symmetry is broken, it is not reflected in the band structure at θ_2 ; the band degeneracy is not lifted (Fig.S3).

¹ Z. Gao and Z. Lan, Phys. Rev. B **102**, 245133 (2020).

² S. K. Kim and J. Zang, Phys. Rev. B **92**, 205106 (2015).

³ M. Koshino, T. Morimoto, and M. Sato, Phys. Rev. B **90**, 115207 (2014).